Eur. Phys. J. B **22**, 37–42 (2001)

THE EUROPEAN PHYSICAL JOURNAL B

EDP Sciences

Imperfect nesting and Peierls instability for a two-dimensional tight-binding model

Q. Yuan[1,2,a], T. Nunner[1], and T. Kopp[1]

[1] Experimentalphysik VI, Universität Augsburg, 86135 Augsburg, Germany
[2] Pohl Institute of Solid State Physics, Tongji University, Shanghai 200092, PR China

Received 22 December 2000

Abstract. Based on a half-filled two-dimensional tight-binding model with nearest-neighbour and next nearest-neighbour hopping the effect of imperfect Fermi surface nesting on the Peierls instability is studied at zero temperature. Two dimerization patterns corresponding to a phonon vector (π, π) are considered. It is found that the Peierls instability will be suppressed with an increase of next nearest-neighbour hopping which characterizes the nesting deviation. First and second order transitions to a homogeneous state are possible. The competition between the two dimerized states is discussed.

PACS. 71.45.Lr Charge-density-wave systems – 63.20.Kr Phonon-electron and phonon-phonon interactions

1 Introduction

The low dimensional electronic materials are known to be very susceptible to a Peierls instability towards a charge density wave (CDW) state driven by the electron-phonon interaction [1]. The presence of a lattice distortion is usually favorable to lower the electronic energy and once this reduction overcomes the increase of lattice deformation energy the Peierls transition takes place. It has been extensively studied in a lot of quasi-one-dimensional (1D) materials such as organic conjugated polymers $(CH)_x$ [2] or inorganic blue bronzes $A_{0.3}MoO_3$ (A = K, Rb, Tl) [3], as well as quasi-two-dimensional (2D) materials such as purple bronzes AMo_6O_{17} (A = Na, K, Tl) [3–5] and monophosphate tungsten bronzes $(PO_2)_4(WO_3)_{2m}$ $(4 \leq m \leq 14)$ [6,7].

It is believed that for the Peierls transition the structure of the Fermi surface (FS) plays an essential role. In ideal 1D systems, the FS, being composed of two points separated by $2k_F$ (Fermi wave vector), is always perfectly nested. The lattice distortion opens a gap at the Fermi level with the consequence that the energy gain from the electronic energy is always dominant, so that the Peierls instability with a metal-insulator transition always takes place (if quantum effects of phonons are not considered [8]).

The situation becomes richer in two dimensions because of a more complex FS structure. In general, the FS is not nested, *i.e.*, a single mode of lattice distortion can connect only two points in the FS, and the gain of electronic energy from this distortion is not enough to overcome the increase of lattice energy. However, in some special cases the FS is still nested and the electronic energy may be lowered substantially by the lattice distortion even if a gap may be not fully opened at the FS as in one dimension. The simplest realization is the 2D square lattice tight-binding model with only nearest-neighbour (n.n.) hopping at half-filling, *i.e.*, the 2D version of the well-known Su-Schrieffer-Heeger (SSH) model [9]. In this case the FS consists of parallel straight lines: $|k_x| + |k_y| = \pi$ as illustrated in Figure 1 by the solid line. One of the Fermi lines may be completely moved to another by a translational vector $Q = (\pi, \pi)$, *i.e.*, the FS is perfectly nested with nesting

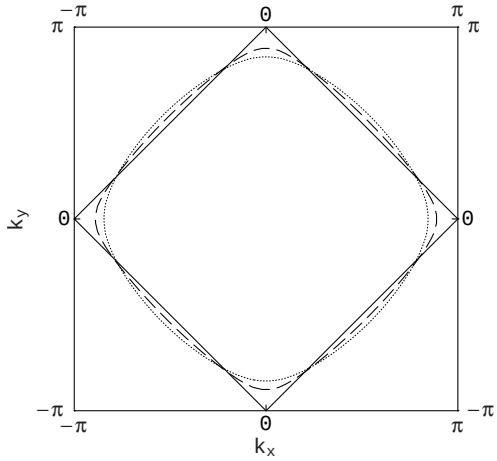

Fig. 1. The Fermi surfaces for the 2D tight-binding model without dimerization at half-filling. The solid line has $t' = 0$, the dashed line has $t' = 0.1$, and the dotted line has $t' = 0.2$.

[a] e-mail: qingshan.yuan@physik.uni-augsburg.de

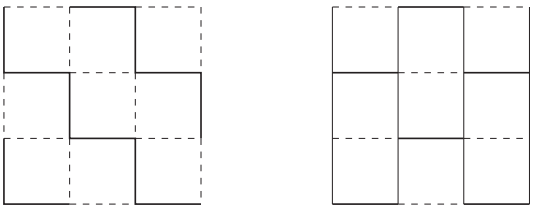

(a) (b)

Fig. 2. The lattice distortion patterns (a) and (b). In the figure a thick solid line corresponds to a strong bond with hopping integral $t(1+\delta)$, a dashed line corresponds to a weak bond with hopping integral $t(1-\delta)$, and a thin solid line corresponds to a normal bond with hopping integral t. Both patterns correspond to phonons with wave vector (π,π). The dimerization is along two axes for case (a), while only along x axis for case (b).

vector Q. The Peierls instability for this model was theoretically studied one decade ago in connection to high T_c superconductors [10,11]. Unlike in one dimension, there are several possible alternation patterns for the lattice distortion and the corresponding bond hopping, as discussed by Tang and Hirsch [10]. In Figure 2 two possible dimerization patterns are shown. Both of them correspond to phonons with wave vector (π,π), which is exactly Q so that the reduced Brillouin zone boundary after distortion perfectly meets the original FS. The difference between them is that for case (a) the dimerization is in both directions, while it is only in one direction for case (b). It was found that even arbitrarily small electron-lattice coupling strength will induce a lattice distortion into case (a) or (b), *i.e.*, the Peierls instability is sure to occur even for this 2D model [10,11]. On the other hand, however, it may be noticed that the present perfect nesting of the FS may be easily broken, for example, by introducing next nearest-neighbour (n.n.n.) hopping which is often not negligible. Then the following problem naturally arises: does the above Peierls instability still survive the imperfect nesting of the FS?

Actually, for those quasi-2D materials which show a Peierls instability perfect nesting of their Fermi surfaces is never present, but an approximate, so called hidden nesting exists [12]. Also, it may be reasonable to expect that the Peierls instability will be suppressed if the FS is so far away from nesting that even no hidden nesting is present. As far as real materials are concerned the shapes of the Fermi surfaces are obtained by band structure calculations and may be often rather complicated. Nevertheless, the tight-binding model with the n.n. and n.n.n. hopping should already be sufficient to simulate an essential property of real Fermi surfaces: whether they are nesting or not. Thus it is necessary to clarify how sensitive the Peierls instability is to the deviations of the FS from perfect nesting which is controlled by n.n.n. hopping. This is the topic addressed in this paper. A similar problem was studied previously by Lin *et al.* [13], however, their study was only limited to the dimerization pattern (a). (Actually this pattern is not favorable in a large region of t' as will be seen later.) We will include the two possible patterns (a) and (b) and address the unexpected competition between them.

2 FS nesting and Peierls instability

We begin with the following Hamiltonian based on a square lattice with a half-filled band:

$$\begin{aligned} H = & -t\sum_{i,j,\sigma}[1+\alpha(u^x_{i,j}-u^x_{i+1,j})](c^\dagger_{i,j,\sigma}c_{i+1,j,\sigma}+\text{h.c.}) \\ & -t\sum_{i,j,\sigma}[1+\alpha(u^y_{i,j}-u^y_{i,j+1})](c^\dagger_{i,j,\sigma}c_{i,j+1,\sigma}+\text{h.c.}) \\ & -t'\sum_{i,j,\sigma}(c^\dagger_{i,j,\sigma}c_{i+1,j+1,\sigma}+c^\dagger_{i,j,\sigma}c_{i+1,j-1,\sigma}+\text{h.c.}) \\ & +\frac{K}{2}\sum_{i,j}[(u^x_{i,j}-u^x_{i+1,j})^2+(u^y_{i,j}-u^y_{i,j+1})^2], \end{aligned} \tag{1}$$

where $c^\dagger_{i,j,\sigma}(c_{i,j,\sigma})$ denotes the creation (annihilation) operator for an electron at site (i,j) with spin σ (i denotes x coordinate and j denotes y coordinate), $u^{x/y}_{i,j}$ represents the displacement component of site (i,j) in x/y direction, t, t' are n.n and n.n.n. hopping parameters and α is the electron-lattice coupling constant. The last term above describes the lattice elastic potential energy with K the elastic constant. The lattice kinetic energy is omitted here since we do not study the dynamic behavior of phonons. For the lattice distortion patterns investigated here, the distance between n.n.n. sites remains unchanged, therefore no dimerization of t' is considered in Hamiltonian (1).

The lattice distortion, as shown in Figure 2 having the wave vector Q, may be explicitly introduced as

$$u^x_{i,j}-u^x_{i+1,j}=(-1)^{i+j}u, \qquad u^y_{i,j}-u^y_{i,j+1}=(-1)^{i+j}u$$

for case (a), and

$$u^x_{i,j}-u^x_{i+1,j}=(-1)^{i+j}u, \qquad u^y_{i,j}-u^y_{i,j+1}=0$$

for case (b), where u is the amplitude of dimerization determined by minimization of the ground state energy. For convenience, two dimensionless parameters are defined as follows: the dimerization amplitude $\delta=\alpha u$ and the electron-lattice coupling constant $\eta=\alpha^2 t/K$. The n.n. hopping integral t is taken as the energy unit.

Before proceeding, we would like to mention that two further possible lattice distortion patterns as discussed in previous works on the 2D Peierls instability, which correspond to wave vector $(\pi,0)$ and/or $(0,\pi)$ [10], are excluded in our study. We omit them because at $t'=0$ their energy gains are much smaller than those for the patterns considered here [10]. (They are possibly favorable only when a large Hubbard U term is switched on [10].) This is physically understandable: they have a different wave vector from the nesting one. Very recently, a more complex lattice distortion pattern with incommensurate structure was studied by Ono and Hamano in the case of

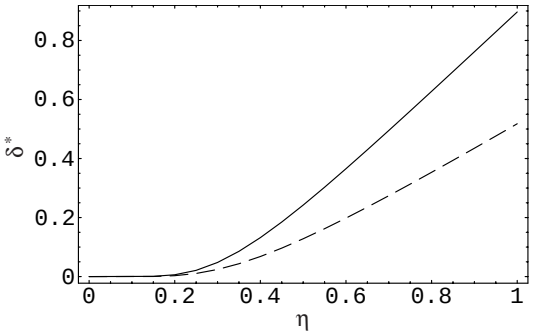

Fig. 3. The optimal value δ^* as a function of η for $t' = 0$. The dashed line is for case (a) and the solid line is for case (b).

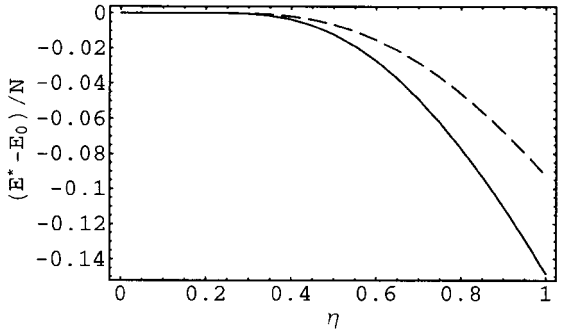

Fig. 4. The energy gain of the dimerized state: E^* at $\delta = \delta^*$ minus E_0 at $\delta = 0$ as a function of η, corresponding to Figure 3.

$t' = 0$ [14]. However it will not be included here since it is not unique [14]. The patterns considered in Figure 2 may be regarded as typical structures for the study of the Peierls instability in two dimensions. In the following the Peierls instabilities for $t' = 0$ and $t' \neq 0$ are discussed respectively.

2.1 t' = 0

For completeness, we first reproduce the results for the perfect nesting case $t' = 0$, which are straightforward but helpful. In momentum space the electronic spectra for case (a) and (b) are respectively written as

$$\varepsilon^{\pm}_{\mathbf{k},\mathrm{a}} = \pm 2\sqrt{(\cos k_x + \cos k_y)^2 + \delta^2(\sin k_x + \sin k_y)^2}\ ,$$
$$\varepsilon^{\pm}_{\mathbf{k},\mathrm{b}} = \pm 2\sqrt{(\cos k_x + \cos k_y)^2 + \delta^2 \sin^2 k_x}\ . \qquad (2)$$

In the ground state only the lower band is fully occupied for each case (*i.e.*, the chemical potential is zero). Then the ground state energy is given by

$$E = 2\sum_{\mathbf{k}} \varepsilon^{-}_{\mathbf{k},\mathrm{a}} + N\delta^2/\eta$$

for case (a), and

$$E = 2\sum_{\mathbf{k}} \varepsilon^{-}_{\mathbf{k},\mathrm{b}} + N\delta^2/2\eta$$

for case (b), where the summation is over the wave vector $\mathbf{k} = (k_x, k_y)$ in the Brillouin zone $-\pi < k_x \pm k_y \leq \pi$ and N is the total number of lattice sites. The factor 2 in front of the summation is due to spin degeneracy. Obviously the increase of elastic energy for case (a) is twice of that for case (b) under the same dimerization δ. For case (a) the energy has explicit analytic expression: $E/N = -\frac{16}{\pi^2}\mathbf{E}(\sqrt{1-\delta^2}) + \delta^2/\eta$, where $\mathbf{E}$ is the complete elliptic integral of the second kind.

The results are shown in Figures 3 and 4. In Figure 3 the optimal dimerization parameter δ^* with lowest energy *vs.* the electron-lattice coupling η is plotted, and Figure 4 gives the corresponding ground state energies E^* at these δ^* values (with respect to the energy of the undimerized lattice E_0 which is equal to $-16/\pi^2$ times N). From these figures it can be seen that the Peierls instability takes place as long as the electron-lattice coupling is non-zero for either case (a) or (b). Although the magnitude of δ^* is small when $\eta \to 0$, it is proven to be finite, with an exponential dependence of $\exp(-c/\eta)$ on η (c is a constant). This confirms the related statement made in the Introduction. Moreover, it is seen from Figure 4 that the energy E^* for case (b) (solid line) is always lower than the corresponding one for case (a) (dashed line) in the full region of finite η, which means that the case (b) is the more favorable dimerization pattern for $t' = 0$. Unfortunately in their works, Mazumdar as well as Tang and Hirsch incorrectly preferred case (a), see reference [11]. A similar conclusion as ours was reached by Ono and Hamano [14].

2.2 t' ≠ 0

For $t' \neq 0$ the perfect nesting of the FS is broken. In Figure 1 the Fermi surfaces for the undimerized lattice are plotted for several t' values. One may see that the bigger t' is the farther the FS deviates from perfect nesting.

Still the Hamiltonian can be easily diagonalized, but the final results are quite nontrivial. Now the electronic spectra become

$$\varepsilon^{\pm}_{\mathbf{k},\mathrm{a}} = -4t'\cos k_x \cos k_y \pm 2\sqrt{(\cos k_x + \cos k_y)^2 + \delta^2(\sin k_x + \sin k_y)^2}\ ,$$
$$\varepsilon^{\pm}_{\mathbf{k},\mathrm{b}} = -4t'\cos k_x \cos k_y \pm 2\sqrt{(\cos k_x + \cos k_y)^2 + \delta^2 \sin^2 k_x}\ , \qquad (3)$$

and the ground state energy is

$$E = 2\sum_{\varepsilon^{\pm}_{\mathbf{k},\mathrm{a}} \leq \mu_{\mathrm{a}}} \varepsilon^{\pm}_{\mathbf{k},\mathrm{a}} + N\delta^2/\eta$$

for case (a), and

$$E = 2\sum_{\varepsilon^{\pm}_{\mathbf{k},\mathrm{b}} \leq \mu_{\mathrm{b}}} \varepsilon^{\pm}_{\mathbf{k},\mathrm{b}} + N\delta^2/2\eta$$

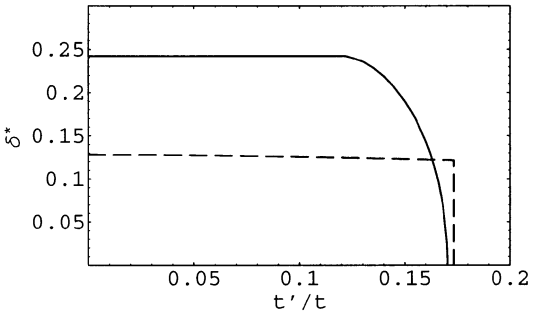

Fig. 5. The optimal value δ^* as a function of t' for $\eta = 0.5$. The dashed line is for case (a) and the solid line is for case (b).

for case (b), where $\mu_{\rm a}$ and $\mu_{\rm b}$ are chemical potentials for case (a) and (b), respectively. By solving the equation $\partial E/\partial\delta = 0$ we may single out the optimal value δ^* for each t' with fixed η. In the following a typical value $\eta = 0.5$ is adopted [13,14].

The results for δ^* are shown in Figure 5. It is clearly seen that δ^* goes to zero with increase of t' in both cases, which means that the Peierls instability is suppressed at some t', as expected. And more interestingly, the details for both cases are different. For case (a) δ^* first decreases weakly with increase of t', but at some critical $t'_{\rm c,1} \simeq 0.1733$, it drops suddenly to zero, showing a first-order transition. On the other hand, for case (b) δ^* first retains its $t' = 0$ value, and after t' is beyond about 0.12 it begins to decrease gradually and approaches zero smoothly at $t'_{\rm c,2} \simeq 0.1704$ – the transition is of second-order. The value $t'_{\rm c,2}$ is close to, but different from $t'_{\rm c,1}$.

To see the above transitions more clearly, we plot in Figures 6 and 7 the dependence of the ground state energy on the dimerization parameter δ for several different t' values for case (a) and (b), respectively. For case (a) it is seen that when t' approaches the critical value $t'_{\rm c,1}$, the energy E first increases with δ and then decreases towards a minimum, as shown in the inset of Figure 6. Thus this minimum may be only a local one. It is expected that at $t'_{\rm c,1}$ the energy E at such a minimum is the same as that at $\delta = 0$, see the inset. And then once t' is beyond $t'_{\rm c,1}$ the δ value with absolutely lowest energy should be taken zero, *i.e.*, $\delta^* = 0$. So a first-order transition arises. On the other hand, for case (b) the energy E always decreases first with increase of δ until a minimum is reached. So this minimum is actually a global one. It shifts continuously towards zero with increase of t', which explains the second-order transition.

It deserves to point out the physical reason for the constant value of δ^* in the small t' region (about $t' < 0.12$) for case (b). Actually, in this region the two energy bands $\varepsilon^{\pm}_{\mathbf{k},\rm b}$ do not overlap when one takes relatively large δ value like δ^*, so that the lower band $\varepsilon^{-}_{\mathbf{k},\rm b}$ is fully occupied and the upper band $\varepsilon^{+}_{\mathbf{k},\rm b}$ is empty in the ground state. Then the electronic energy is simply given by $\sum_{\mathbf{k}} \varepsilon^{-}_{\mathbf{k},\rm b}$, which is independent of t' due to $\sum_{\mathbf{k}} \cos k_x \cos k_y = 0$. Therefore the ground state energy for $t' \neq 0$ is the same as that

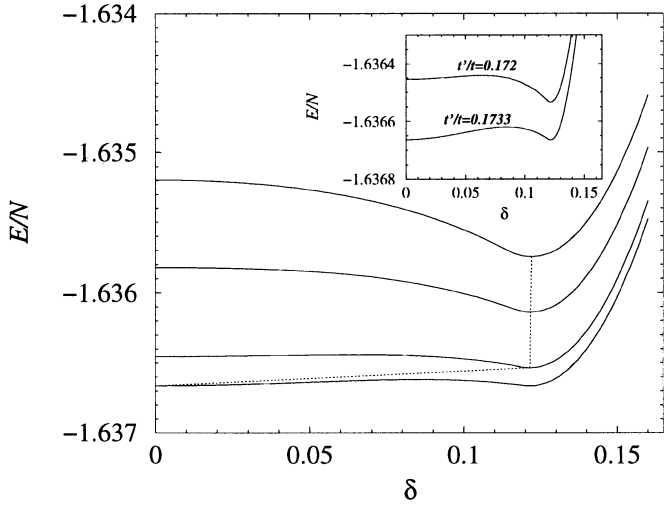

Fig. 6. The ground state energy per site as a function of δ for several t' values for case (a). The solid curves from up to down correspond to $t' = 0.164,\ 0.168,\ 0.172,\ 0.1733$, respectively, and the dotted line connects the global minima of them. The curves for $t' = 0.172$ and $t' = 0.1733$ are enlarged in the inset, where the initial increase in each curve is shown.

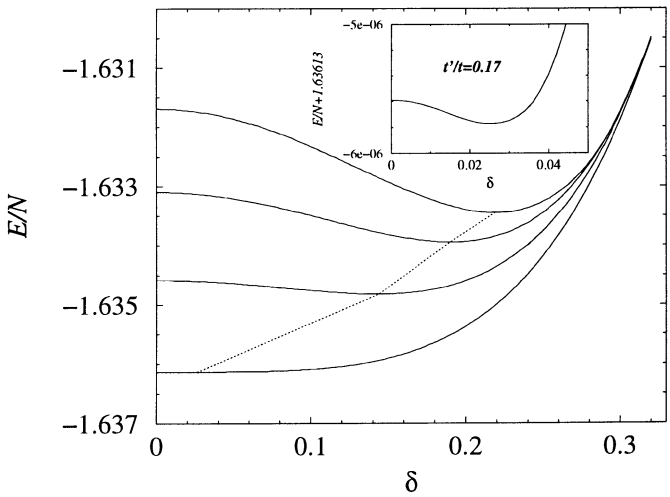

Fig. 7. The same as Figure 6 for case (b). The curves from up to down correspond to $t' = 0.14,\ 0.15,\ 0.16,\ 0.17$, respectively. In the inset the curve for $t' = 0.17$ is shown in the small δ region.

for $t' = 0$, so is the solution δ^*. For more clearness, the electronic spectra for case (b) are plotted in Figure 8 for two different t' values, where the two bands are only found to touch for $t' = 0.1$. We also point out that for case (a) the two bands always overlap for all t' (not shown) because they are identical in the Brillouin zone boundary: $k_x - k_y = \pm\pi$.

While so far the results of the Peierls instabilities for the two patterns have been given separately, it is now natural to think of the competition between them. The competition becomes evident when the respective lowest energies E^* at different t' values are compared, as shown in Figure 9. It is interesting to see that the energy E^* for

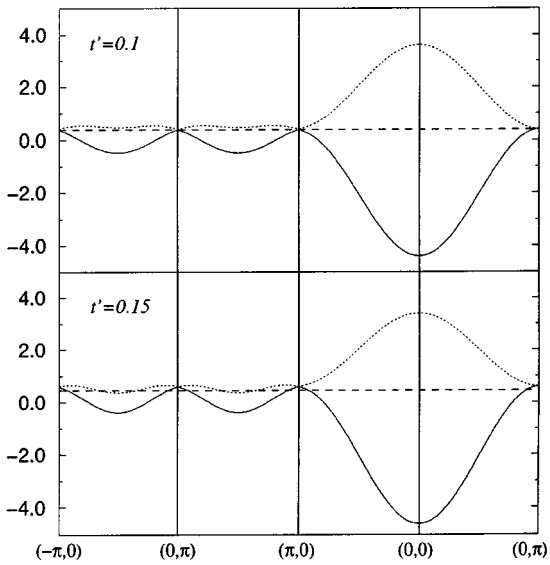

Fig. 8. The electronic spectra for case (b). The solid and dotted curves represent energy bands '−' and '+', respectively, and the dashed horizontal line shows the chemical potential. For $t' = 0.1$, $\delta^* = 0.2422$, $\mu_b = 0.4$, the two bands display no overlap; while for $t' = 0.15$, $\delta^* = 0.19$, $\mu_b = 0.4556$, the two bands are overlapped.

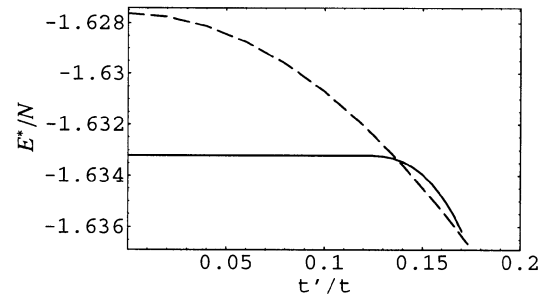

Fig. 9. The energy at $\delta = \delta^*$ as a function of t' for $\eta = 0.5$, corresponding to Figure 5. Both curves stop at their respective critical points.

case (b) is first less than that for case (a), but later becomes larger with increase of t'. Consequently, a transition between these two dimerization patterns is predicted. To summarize, the evolution of the stable state for the system with increase of t' may be described as follows: at $t' = 0$ the dimerized state stabilizes due to the perfect FS nesting, and moreover the dimerization pattern takes form (b). This state remains stable until at some t' value (which is about 0.137 for $\eta = 0.5$) it is replaced by the other dimerized state (a). Finally, the dimerized state breaks down, *i.e.*, the Peierls instability is suppressed at some critical value t'_c which is equal to $t'_{c,1}$ as can be seen in Figure 9. Thus the suppression is a first-order transition.

Above, only the results for $t' > 0$ are presented. Taking $t' \to -t'$ will reflect all the results as shown by Figures 5 and 9 about $t' = 0$. This is because of particle-hole symmetry at half-filling, that is, the Hamiltonian with $-t'$ may be related to that with t' through the particle-hole transformation: $c_{i,j,\sigma} \to (-1)^{i+j} c^\dagger_{i,j,\sigma}$.

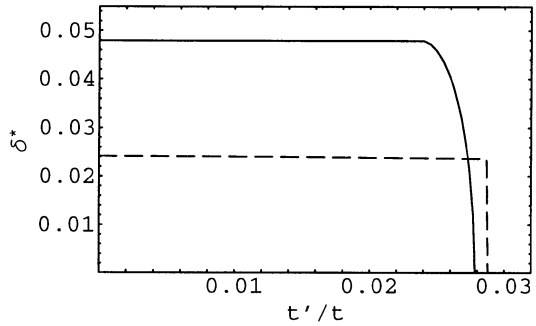

Fig. 10. The same as Figure 5 but with $\eta = 0.3$.

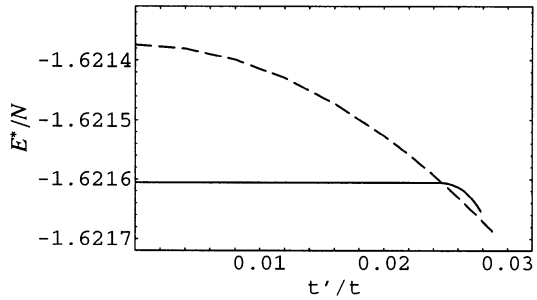

Fig. 11. The same as Figure 9 but with $\eta = 0.3$.

Up to now all results have been shown for fixed η. In the last part of this section we will look at the role of η. Since the parameter η only appears in the elastic energy, *i.e.*, it is irrelevant to the electronic part of the ground state energy, the qualitative properties of curves E *vs.* δ as shown in Figures 6 and 7 are expected to be retained, so are the above qualitative results for the Peierls instability. Quantitatively one may think, the smaller the electron-lattice coupling η is (or equivalently the larger the elastic strength K is), the smaller the critical value t'_c for the suppression of the Peierls instability should be. As a check, the case for $\eta = 0.3$ is calculated. The results are shown in Figures 10 and 11, which are consistent with the above predictions. Also note that the critical value t'_c drops fast with decreasing η.

3 Discussion

In the previous section the Peierls instability for two dimerization patterns has been carefully studied in its dependence on t'. The results are instructive. It is now known that low-dimensional metals show two types of electronic instabilities: either a Peierls instability or a superconducting one. The Peierls instability may prevent some metals from entering a superconducting state. For example, in the transition metal bronzes, the Peierls instability is the dominant mechanism and superconductivity was seldom found [6]. Our results suggest that the Peierls instability may be suppressed by some way of increasing imperfect nesting, for example, by applying pressure to

enhance the n.n.n. hopping. Moreover, the possible transition between different dimerized states is reminiscent of the experimental results in monophosphate tungsten bronzes like $P_4W_{12}O_{44}$, where double Peierls transitions occur with change of temperature [6,7]. The competition between two dimerization patterns at finite temperatures is believed to be interesting and will be left for future investigation.

A further problem is the consideration of effects of electron correlations, *e.g.*, the Hubbard U term which are not included in this work. For $t' = 0$ the problem has been studied by Tang and Hirsch by numerical calculations [10,11]. It was found that the on-site Coulomb interaction weakens the dimerization in two dimensions as soon as U is present [11]. The possible explanation is that the U term favors the appearance of antiferromagnetic (AF) spin order in 2D half-filled Hubbard model, while the dimerization stabilizes local spin singlets which are unfavorable for strong U. Above, we showed that t' also suppresses dimerization. Does this indicate that the simultaneous presence of both U and t' will speed the suppression of the dimerization? We leave this issue for future work and only give some clues here from previous analysis in the large U limit (for the moment the concrete dimerization pattern is not considered). In this limit we are facing a problem of localized electrons interacting *via* an effective n.n. exchange J ($\sim t^2/U$) and n.n.n. exchange J' ($\sim t'^2/U$). The Peierls system then transforms into the corresponding spin-Peierls (SP) system. The 2D (or quasi-1D) spin-Peierls instability without n.n.n. exchange J' was studied by some authors [15–17]. It was found that the SP transition does not spontaneously occur unless the so called spin-lattice coupling (analogous to η here) exceeds a threshold. On the other hand, it was known that the n.n.n. exchange J' will frustrate the AF order for the 2D spin system. So one may assume that the additional inclusion of J' will be favorable to the formation of a SP state. Thus it is not unreasonable to believe that the effects of t' and U on the Peierls instability may cancel in part when acting simultaneously, although each of them separately tends to suppress it.

4 Conclusion

In conclusion, a 2D tight-binding model with n.n. hopping t and n.n.n. hopping t' is used to study the effect of imperfect FS nesting on the Peierls instability of the ground state. Two possible dimerization patterns corresponding to a phonon vector (π, π) are considered as case (a) and (b). It is found that the Peierls instability will be suppressed with an increase of t' which characterizes the deviation from perfect nesting. The details for the two cases are different: for case (a) the suppression is a first-order transition while for case (b) it is of second-order. Also a transition between the two dimerized states is investigated.

We acknowledge the financial support by the Deutsche Forschungsgemeinschaft through SFB 484 and the BMBF 13N6918/1. Q. Yuan also acknowledges the support by the Chinese NSF.

References

1. G. Grüner, *Density Waves in Solids* (Addison-Wesley, Redwood City, 1994).
2. *Organic Conductors*, edited by J.P. Farges (Marcel Dekker, New York, 1994).
3. *Physics and Chemistry of Low-Dimensional Inorganic Conductors, NATO ASI Series B: Physics*, Vol. 354, edited by C. Schlenker, J. Dumas, M. Greenblatt, S. van Smaalen (Plenum, New York, 1996).
4. J. Dumas, C. Schlenker, Int. J. Mod. Phys. B **7**, 4045 (1993).
5. X.K. Qin, J. Shi, H.Y. Gong, M.L. Tian, J.Y. Wei, H. Chen, D.C. Tian, Phys. Rev. B **53**, 15538 (1996); R. Xiong, Q.M. Xiao, J. Shi, H.L. Liu, W.F. Tang, M.L. Tian, D.C. Tian, Mod. Phys. Lett. B **14**, 345 (2000).
6. C. Schlenker, C. Hess, C. Le Touze, J. Dumas, J. Phys. I France **6**, 2061 (1996).
7. E. Wang, M. Greenblatt, I.E. Rachidi, E. Canadell, M.H. Whangbo, S. Vadlamannati, Phys. Rev. B **39**, 12969 (1989); S. Drouard, D. Groult, J. Dumas, R. Buder, C. Schlenker, Eur. Phys. J. B **16**, 593 (2000).
8. For the study on the effects of quantum lattice fluctuations, see *e.g.*, H. Zheng, Phys. Rev. B **50**, 6717 (1994).
9. A.J. Heeger, S. Kivelson, J.R. Schrieffer, W.P. Su, Rev. Mod. Phys. **60**, 781 (1988).
10. S. Tang, J.E. Hirsch, Phys. Rev. B **37**, 9546 (1988).
11. S. Mazumdar, Phys. Rev. B **39**, 12324 (1989); S. Tang, J.E. Hirsch, Phys. Rev. B **39**, 12327 (1989).
12. M.H. Whangbo, E. Canadell, P. Foury, J.P. Pouget, Science **252**, 96 (1991).
13. F. Lin, X.B. Chen, R.T. Fu, X. Sun, Y. Kawazoe, Phys. Stat. Sol. (b) **206**, 559 (1998).
14. Y. Ono, T. Hamano, J. Phys. Soc. Jpn **69**, 1769 (2000).
15. F.C. Zhang, P. Prelovsek, Phys. Rev. B **37**, 1569 (1988).
16. S. Inagaki, H. Fukuyama, J. Phys. Soc. Jpn **52**, 3620 (1983).
17. Q.S. Yuan, Y.M. Zhang, H. Chen, Phys. Rev. B **64**, 012414 (2001), `cond-mat/9911119`.